PROCEEDINGS OF THE ROYAL SOCIETY A MATHEMATICAL, PHYSICAL & ENGINEERING SCIENCES

On Low-Gravity Droplet Combustion

C. T. Avedisian, J. C. Yang and C. H. Wang

Proc. R. Soc. Lond. A 1988 **420**, doi: 10.1098/rspa.1988.0123, published 8 November 1988

Proc. R. Soc. Lond. A **420**, 183–200 (1988)
Printed in Great Britain

On low-gravity droplet combustion

By C. T. Avedisian, J. C. Yang and C. H. Wang†
Sibley School of Mechanical and Aerospace Engineering, Cornell University, Ithaca, New York 14853-7501, *U.S.A.*

(*Communicated by F. J. Weinberg, F.R.S. – Received* 4 *March* 1988)

[Plates 1–3]

An experimental method is described for studying the combustion of a stationary unsupported fuel droplet in a stagnant ambience under very low gravity. A unique feature of the method is that of being able to observe the droplet burning history over the entire period from ignition to extinction or complete burning. The procedure consisted of propelling a droplet from a piezoelectric generator in a near vertical trajectory and then releasing the chamber within which the droplet was introduced, as well as associated instrumentation, into free fall when the droplet reached the apex of its trajectory. Results with the technique are described for toluene and heptane droplets.

A phenomenon believed to be indicative of extinction was observed for an unsupported heptane droplet, whereas the evidence for extinction of toluene was less clear. Measured burning rates were in good agreement with both early theories that have assumed spherically symmetric combustion, and with prior limited experiments on heptane droplets obtained under low gravity that, however, were capable of recording a more limited fraction of the total burning history.

1. Introduction

The absence of free or forced convective gas flow around a burning droplet simplifies the mechanisms governing its combustion. The velocity field around the droplet is radially symmetric and energy transfer is only by conduction, radiation, and Stefan-type convection. Such conditions are typically encountered in practice within a spacecraft environment. The attractiveness of neglecting vapour flow around a burning droplet in model development belies the difficulties of devising a ground-based experiment that renders valid this assumption. This paper describes an experimental method for studying the combustion of free (unsupported) and nearly stationary droplets of liquid fuels at low gravity. That the droplets should be unsupported was recognized as being essential for avoiding the possible effects of an artificial protuberance, such as a support fibre, on the droplet burning rate: droplets in a realistic environment are not hanging from fibres but are free floating.

† Permanent address: Department of Mechanical Engineering, National Taiwan University, Taipei, Taiwan; formerly Visiting Scientist at Cornell University.

The experimental method was based on the drop tower. In this experiment a test droplet, its enclosed environment (i.e. the combustion chamber within which the droplet is contained), and associated instrumentation were simultaneously released into free fall. During the fall, the droplet was ignited and its burning history was recorded by high-speed cine photography. The gravity experienced by the droplet is commensurate with the drag on the falling package. For free fall in a vacuum, for which there will be no drag around the falling package, the gravity level in the moving frame of reference is zero. An object falling in air will experience a proportionately larger gravity level, the precise magnitude of which depends on the shape of the object and the prevailing air properties. Gravity levels that characterized the present experiment were on the order of $10^{-3} g_0$.

The experimental method is demonstrated by reporting the evolution of droplet diameter and flame shapes for two model hydrocarbon fuels burning in air under a pressure of 0.101 MPa: *n*-heptane and toluene. Heptane was selected because of its extensive use in other prior droplet burning experiments, thus facilitating comparisons with such measurements as the droplet burning rate and evolution of droplet diameter. The particularly luminous flames produced by toluene droplets enabled photographically recording their flame shapes. A feature of the method described here is that the complete unsupported droplet burning history, from ignition to burnout or extinction, could be recorded under low gravity.

Nomenclature

C_p	specific heat
$d(t)$	instantaneous droplet diameter
d_0	initial droplet diameter
D	$\equiv d/d_0$
g	gravitational constant
g_0	Earth normal gravity (980 cm s^{-2})
Gr_0	Grashof number ($\equiv g\beta(T_f - T_\infty) d_0^3 \rho_g^2/\mu_g^2$)
h_{fg}	heat of vaporization
k_g	vapour thermal conductivity
Q	heat of combustion
Re_0	Reynolds number ($\equiv v(t) d_0 \rho_g/\mu_g$)
t	time
T_b	normal boiling point
T_∞	far field gas temperature (=298 K)
$v(t)$	instantaneous droplet velocity
W_f	fuel molecular mass
W_o	oxygen molecular mass
$Y_{r\infty}$	ambient oxygen mass fraction (=0.232)
β	isothermal compressibility
ρ_g	vapour density
ρ_l	liquid density
μ_g	vapour viscosity
τ	$\equiv t/(\rho_l C_p d_0^2/k_g)$

2. Review of prior work

The idea of dropping objects from preselected heights to simulate zero gravity conditions in the frame of reference of the falling object goes back to the time of Galileo and his experiments using the Leaning Tower of Pisa. The modern forerunner of this approach is the 'drop tower' the basic elements of which are as configured in the present study and described in §3. The method was first used to study the burning of liquid droplets by Kumagai (1956) and Kumagai & Isoda (1957). Employing a free-fall distance of 4.9 m the spark ignited burning of isolated droplets of ethanol and *n*-heptane of about 1 mm initial diameter that were hanging from a silica fibre under a pressure of 0.101 MPa was studied. Additional studies have also employed fibre-mounted droplets (or solid particles) to study the burning at low gravity of such fuels as single component hydrocarbon liquids, coal particles, and emulsified liquids (Isoda & Kumagai 1959; Faeth *et al.* 1969; Lazar & Faeth 1971; Okajima & Kumagai 1982; Gieras *et al.* 1985; Okajima *et al.* 1985; Gieras *et al.* 1986; Kimura *et al.* 1986). Effective gravity levels experienced within the moving frame of reference are believed to be in the range of $10^{-2}\,g_0$ to $10^{-5}\,g_0$.

The above studies employed suspended droplets and are thus open to the criticism typically directed at data obtained by using droplets hanging from fibres: ambiguities in defining the droplet shape because of its distortion by the fibre, possible alterations of the heat transfer rate to the droplets because of heat conduction through the fibre, and effects on internal bubbling and nucleation mechanisms within the droplet caused by the fibre acting as an extraneous nucleation aid. Nevertheless, there is no question that the information obtained from experiments which have used droplets hanging from fibres have in the main provided a firm foundation upon which our present understanding of the theory of droplet burning rests. The problem, though, is that one does not know *a priori* what the precise effects of a fibre would be unless one has observed the behaviour of unsupported droplets under similar conditions.

A difficulty in using the drop tower to study an unsupported droplet concerns coordinating the release of the droplet in the falling package itself, and/or using droplets that are small enough that they will completely burn within the experimental time available. If the critical timing necessary to captivate a droplet cannot be resolved, a relative motion will exist between the droplet and instrumentation package with the result being that the droplet could drift out of the field of view of the camera before burnout; if the droplet is too large, the experiment will be terminated by the instrumentation package impacting the shock absorber before the droplet completely burns.

Six studies have been reported that employed the drop tower to study burning of an unsupported liquid droplet at low gravity (Kumagai *et al.* 1971; Okajima & Kumagai 1975; Brzustowski *et al.* 1979; Knight & Williams 1980; Brzustowski *et al.* 1981; Shaw *et al.* 1987). All of them involved first holding captive a droplet by one or more fibres and then freeing the droplet by a jerking motion of the fibre along the axis of the fibre. In these studies, either the initial droplet diameters (being typically greater than 1 mm diameter) were too large for the liquids used

for complete burning to occur within the experimental time available (ranging from 1 to 2.2 s), or the critical timing necessary to captivate the droplet by releasing the instrumentation package at the correct instant after disengagement of the droplet from the support fibre could not be resolved so that the droplet drifted out of the field of view of the camera during the period of free fall.

The key to observing a greater fraction of the total droplet burning time lies both in improving the reliability of the droplet generation technique and in using smaller droplets. In the following we describe an experimental method in which a small unsupported droplet (of the order of 500 μm initial diameter) was generated by a different method from that previously used in drop tower experiments. The technique permits observation of the entire period of burning from ignition to burnout or extinction.

3. Experiment

3.1. *Introduction*

The experimental method consisted of propelling a test droplet upward in a near vertical trajectory. Levitation in a low-gravity environment was achieved by releasing the instrumentation package when the droplet reached the apex of its upward trajectory. In this respect the idea is similar to that used in several previous studies. The major difference is in the manner of creating the free drop and in the repeatability of the droplet trajectory from run to run.

A droplet generator, described below, was used to generate a steady continuous stream of droplets in a near vertical trajectory and then shut off. The last droplet emerging from the nozzle was the one studied. When this droplet reached the apex of its upward trajectory, it was ignited by a spark from electrodes positioned adjacent to the apex and the instrumentation package was released into free fall. In this way the droplet was effectively captured with at most a small velocity (usually less than 10 mm s^{-1} corresponding to a droplet Reynolds number less than 0.01) that was created by inaccuracies in timing the release of the platform with the time of flight of the droplet to its apex, or perhaps by the impulse imparted to the droplet by the spark. These inaccuracies were minimized by the method of droplet generation used and the timing electronics developed. The success of the method was evidenced by the high-speed photographic record which captured droplets, some which were motionless, that stayed within the field of view of the camera for the entire period of combustion from ignition to burnout or extinction.

Figure 1 illustrates a schematic diagram of the principle of operation. The continuous stream of droplets created from the generator, only the nozzle of which is illustrated in figure 1, produces a parabolic trajectory of droplets. The height of the droplet trajectory will depend on the initial velocity of the droplets at the nozzle exit and the trajectory angle θ. During the flight of the droplets the component of velocity in the vertical direction of each droplet will decrease and vanish precisely at the apex. At the apex the only motion of the droplet is horizontal. The droplet then begins its downward flight from the apex with a velocity corresponding to that of an object in free fall. If the surrounding and enclosed gas is released into free fall at this instant, as well as the optical

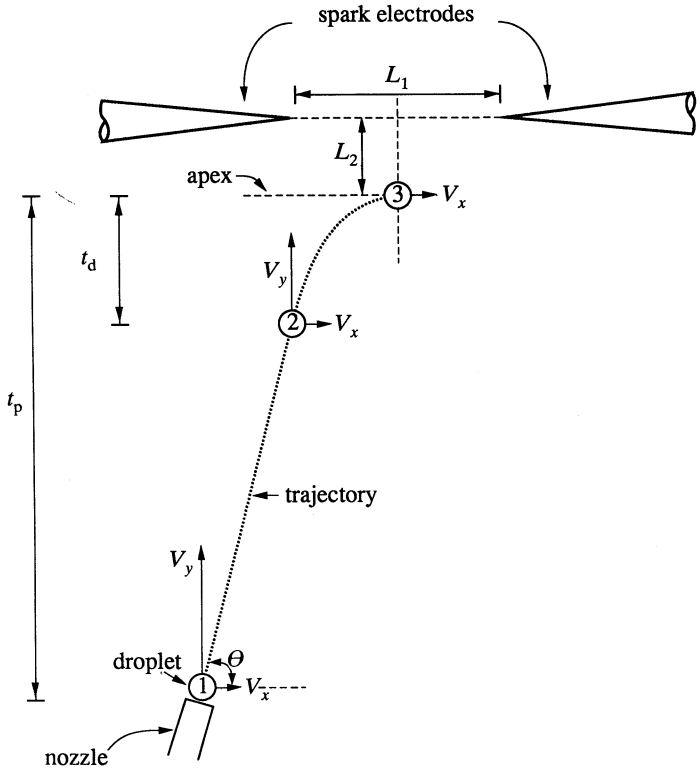

FIGURE 1. Trajectory of the last droplet emerging from the generator. The drop package was released into free fall when this droplet reached the apex, position 3.

instruments positioned at the apex, then the droplet will be effectively motionless with respect to the camera because the gas will also be in rigid body motion, and the droplet will appear levitated. This state of levitation is identical to that which an object in a near-zero gravity field would experience.

Differences between the drag experienced by the falling object and that experienced by the drop within the combustion chamber, which are created by inaccuracies in timing the release of the platform with the droplet reaching the apex of its trajectory, can create a relative motion between the droplet and falling package. The droplet could drift out of the field of view of the camera thus curtailing the period of observation. Such drifting was apparently responsible for the inability to observe a burning droplet over the entire period of combustion from ignition to burnout in several of the previously reported free droplet studies discussed in §2. The extent of this motion is governed by the aerodynamic shape of the falling package and the free-fall distance; elaborate schemes have been used to compensate for air drag on falling packages in drop tower experiments (see, for example, Knight & Williams 1980; Brzustowski *et al.* 1981). In the present experiments the relatively short free-fall distance (7.6 m) coupled with an improved droplet generation method minimized air drag on the falling package and droplet drift to such an extent that complete combustion of an unsupported droplet could be observed.

3.2. *Description of the apparatus*

A schematic diagram of the overall drop tower facility is illustrated in figure 2. It consisted of (1) a vertical shaft 7.65 m tall, (2) a drop package (figure 3), which measured 0.46 m × 1.22 m × 0.61 m and which contained the droplet generator and optical instruments for a total weight of about 180 kg, (3) an upper work station with moveable floor to expose the drop shaft, (4) deceleration tank, (5) drop package release mechanism, (6) timing control unit, (7) droplet generator, and (8) ignition system. The heart of the system is the droplet generator and timing control unit.

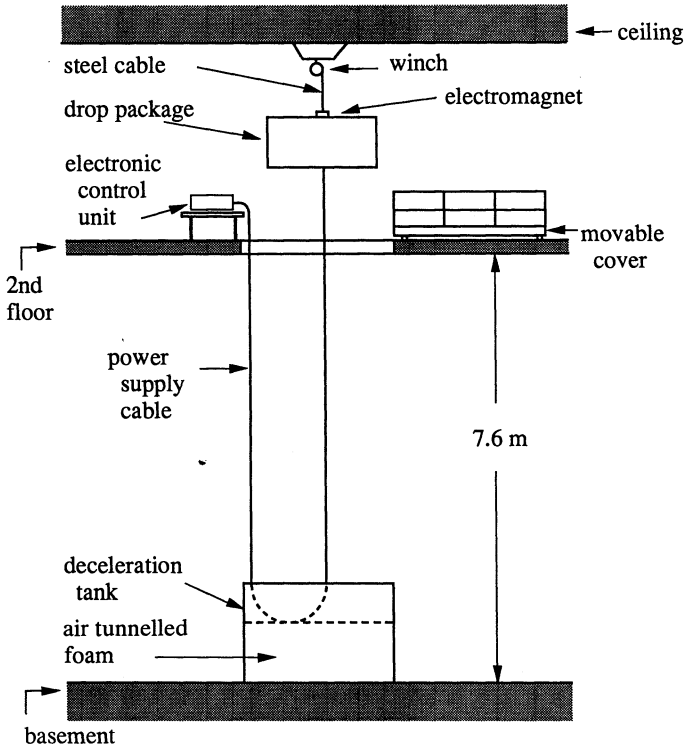

FIGURE 2. Schematic diagram of the drop tower facility (not to scale).

The drop package measured 0.46 m wide, 1.22 m long, and 0.61 m. The bottom consisted of an aluminium plate 5 cm thick on which was mounted the camera, generator, and lighting unit. Several variacs and switches were also placed on the package. The surrounding framework consisted of steel support rods. Power to the on-board units was provided by a single power supply cable (acting like a sort of umbilical cord) that hung from the bottom centre of the package. Little air drag could be attributed to this cable because it was hung from the bottom centre of the aluminium plate. This method was more convenient, and allowed for greater flexibility, than supplying power from batteries mounted directly on the package. The relative positions of the camera, droplet generator, and lighting are illustrated in figure 3.

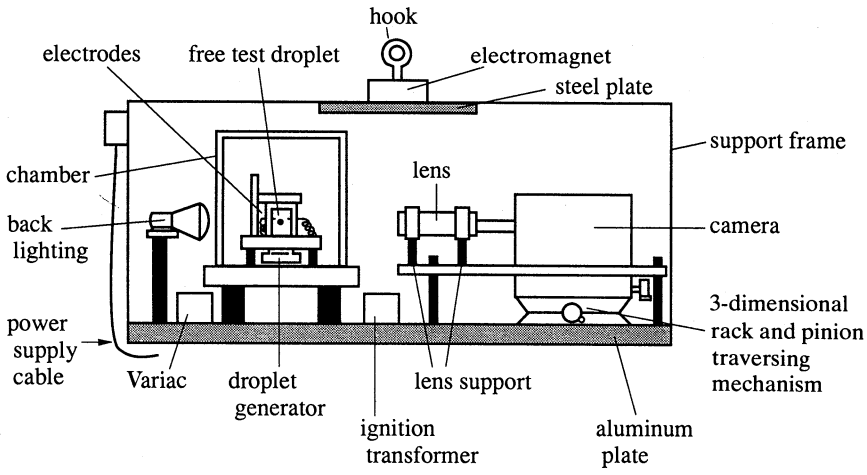

FIGURE 3. Schematic illustration of the drop package.

A measure of the drag experienced by this package during free fall was provided by an accelerometer attached to the package. Figure 4 shows the evolution of gravity over a time period that was characteristically observed for complete burning of the droplets studied. Initially the effective gravity in the moving frame of reference is zero because at the instant of release the velocity of the package is also zero. As free fall proceeds and the package accelerates, the effective gravity level also increases, nearly linearly as shown in figure 4, and reached a maximum of about 0.007 g_0 after 0.4 s (the burning times of the heptane droplets studied) or 0.004 g_0 after 0.25 s (the burning time of a toluene droplet).

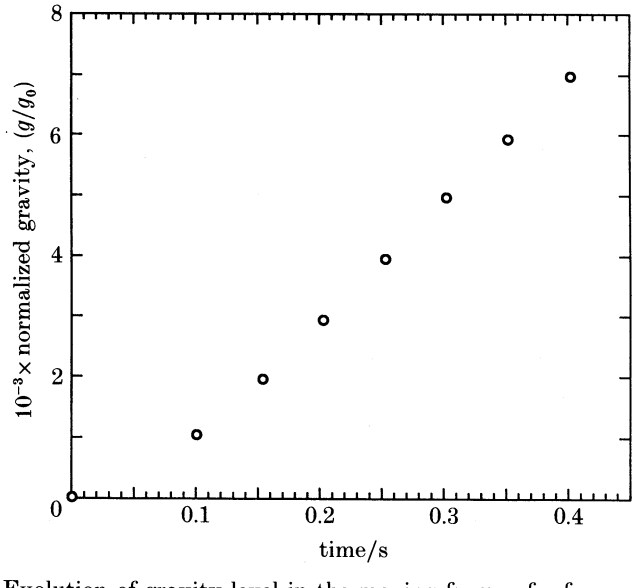

FIGURE 4. Evolution of gravity level in the moving frame of reference; $g_0 = 980$ cm s^{-1}.

The droplet generator was based on the ink-jet method of generating droplets. The design is similar to that used by Wang (1983). Figure 5 is a schematic cross-sectional view of the generator used. It consisted of a piezoelectric transducer, which formed one side of a small chamber to which was attached a glass nozzle. On applying a programmed voltage to the transducer, the transducer deflects and causes a proportionate amount of liquid to be ejected from the nozzle opening. The voltage drive signal used in the present experiment was 50 V with a pulse width of 100 μs. For the 2 mm internal diameter glass nozzles used in the present study, droplets of just under 500 μm diameter were produced; smaller droplets (down to 50 μm diameter) could be generated by using smaller-diameter nozzles. The generator can be operated 'on demand', which basically means that a single droplet could be generated as desired, or continuously thus generating a stream.

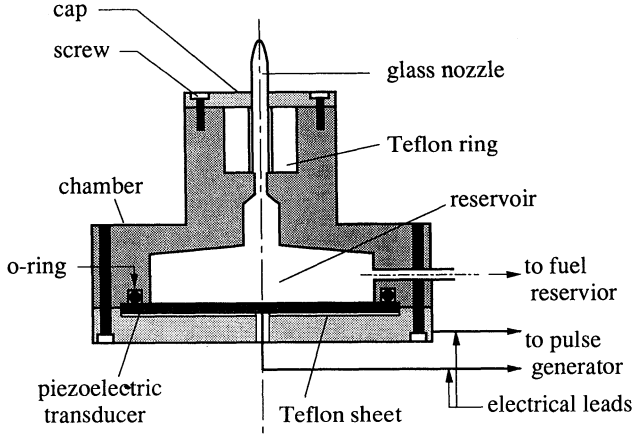

FIGURE 5. Cross-sectional view of the droplet generator (not to scale).

In the present experiments the generator was operated in the continuous mode at a frequency of 2 Hz then shut off. The last droplet emerging from the nozzle was the one studied in an experiment. The rationale for this approach centred around the propensity of air bubbles to be trapped within the nozzle, thus making it very difficult to produce droplets of the same size, initial velocity, and hence time of flight (t_p; see figure 1) of the droplet from the nozzle exit to the apex. The ability to measure accurately t_p *for the droplet studied* was essential for success. The t_p was found to be unique to each stream and was not relevant to the droplet actually studied if the time of flight assigned to that droplet was measured from a stream that was different from that in which it belonged. Such would be the case by simply turning the droplet stream on and measuring t_p, then turning it off, and back on. By generating a continuous stream to measure t_p (and in the process flushing out any air bubbles in the generator), shutting it off, and then performing the experiment on the last droplet generated from *that* stream, the time of flight could be measured for droplets in the same stream within which the particular droplet studied was actually a part of. The trajectory heights were typically about 1.8 cm, and measured times of flights ranged from 60 ms to 64 ms for the droplet

diameters studied. The trajectory angle was not precisely vertical ($\theta = 88°$) to avoid collisions between rising and falling droplets, and collisions between falling droplets and the glass nozzle.

The last droplet emerging from the nozzle was ignited by spark discharge (from an ignition transformer capable of generating up to 10^4 V) across two electrodes positioned slightly above the apex of the droplet trajectory as schematically illustrated in figure 1. The electrodes were sewing needles and stainless steel capillary tubes 0.685 mm diameter and spaced 6.03 mm between their tips. The droplet stream was positioned such that the apex was centred between the electrodes and 0.9 mm below an imaginary line connecting them. The spark was activated at the instant the droplet stream was shut off, and it remained on for approximately 70 ms. This positioning and spark duration was a compromise between minimizing disturbances of the surrounding air by the hot spark, minimizing the impulse imparted by the spark to the droplet, and being able to ignite the drop. If the spark were on too long, the gas surrounding the droplet would be heated with the concomitant natural convective motion created by this heating sweeping the droplet to a higher position than measured from the continuous stream in the absence of the spark. The droplet would then be in motion when the instrumentation package was released and the droplet would drift out of the field of view of the camera before burning was complete. If the spark duration were too short, the droplet would not ignite.

The droplet generator was mounted within a Perspex chamber containing room temperature air at 0.101 MPa. The chamber measured 26 cm high with an 18 cm square cross section; the chamber walls were 0.6 cm thick. The air in this chamber was stationary and effectively in rigid body motion during free fall.

The drop package was initially hung from an electromagnet. Deactivation of the magnet released the package into free fall. This approach was judged to be more convenient than to hang the package from a wire and then to release the package by cutting the wire (Knight & Williams 1980). The intrinsic delay time of deactivation of the magnet (t_d in figure 1) had to be included in the timing release circuit to coordinate the package release with the droplet reaching the apex of its trajectory. This delay was measured to be 24 ms for the magnet used. Power to the magnet was terminated when the droplet reached the generic position labelled as '2' in figure 1, yet the package actually remained attached to the magnet until position '3' (the apex) was reached.

The timing control unit consisted of a pulse generator to drive the droplet generator and a series of cascaded frequency dividers and solid state relays for turning the spark on and off and deactivating the electromagnet. Further details of the circuit are provided elsewhere (Yang 1988).

Direct back lighting was used for recording the droplet burning process. This lighting was provided by a single GTE tungsten halogen projector lamp. Light intensity was varied from that which allowed a clear image of the droplet (for the purpose of measuring the evolution of droplet diameter) to that which permitted the flame to be seen (for illustrating the flame shape around a toluene drop). The camera was a Millikan DBM-55 high speed, high 'g', camera operated at 250 frames per second and equipped with a Bausch & Lomb MonoZoom-7 lens

with a 0.5X objective. Kodak Tri-X reversal film ASA 400) was used. The camera was mounted on a three-dimensional rack and pinion traversing mechanism to facilitate positioning of the camera lens at the apex of the droplet trajectory.

The shock absorber consisted of a cylindrical steel tank 1.8 m in diameter and 1.8 m high. It was filled with two layers of foam rubber, each layer being 0.6 m thick. The upper layer consisted of cross-linking air tunnels and the lower layer was made of solid foam. This design was found to be an effective shock absorber with no bouncing upon impact and with no damage yet having been done to the instruments aboard the drop package.

4. Discussion

A measure of the success which may be expected from the experimental method described in §3 for capturing a free droplet in a nearly levitated state and in a low-gravity free fall condition is provided in figure 6, plate 1. High-speed photographic sequences of burning heptane (figure 6*a*) and toluene (figure 6*b*) droplets with initial diameters of 500 μm and 467 μm are shown. The movie sequences illustrated were obtained by using direct back lighting. The number below each photograph indicates the relative position of that picture in the complete sequence (the time increment between successive frames was 4 ms). The black mark at the top of each frame in figure 6 was created by a protrusion that is attached to the border of the opening on the movie camera through which light enters to expose the film. The mark is thus stationary with respect to the moving frame of reference. As illustrated the droplet diameter decreased until it completely disappeared (for toluene, figure 6*b*) or remained constant (for heptane, figure 6*a*). The very small depth of field (less than 1 mm) coupled with the sharp droplet images shown in figure 6 showed that any droplet motion was essentially two dimensional.

It was almost impossible (except by a random event) to capture a droplet *precisely* at the apex of its upward trajectory. Some motion of the droplet was usually observed for the droplets studied. A measure of the magnitude of the motion is illustrated by comparing the position of the droplet with the camera marker. Movement is clearly shown in figure 6, particularly in figure 6*a* as evidenced by the gradual appearance of the electrode beyond the 38th frame in that sequence (the frames were cut to centralize the droplet within each picture). The toluene droplet (figure 6*b*) exhibited much less motion. The effective Reynolds number of the heptane and toluene droplets, defined as $Re = v(t)\, d(t)\, \rho_g/\mu_g$, is illustrated in figures 7 and 8. The droplet motion is in the Stokes flow régime; the Reynolds numbers were on the order of 0.01 for over 80% of the burning history.

The flame is not visible around the droplets shown in figure 6, though the droplet diameter is clearly visible. The background illumination was too intense for the flame to be visible, especially for heptane, which exhibited a bluish flame. To photograph the flame the light intensity was reduced so that the majority of light to expose the film came from the luminosity of the flame. Figure 9 shows various aspects of the burning sequence of a toluene droplet (a different drop than that illustrated in figure 6*b*): the film was printed on low (figure 9*a*, plate 2) and

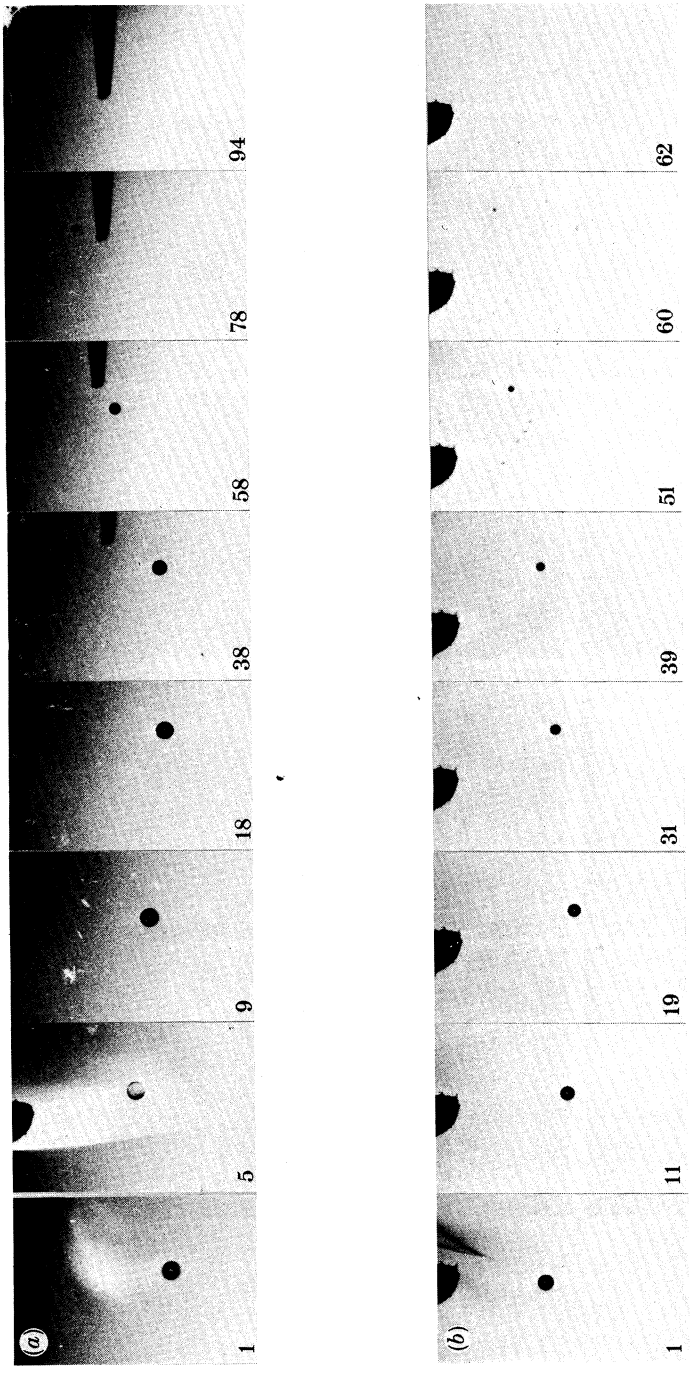

FIGURE 6. Photographic sequences of a burning and free-falling heptane (*a*) and toluene (*b*) droplet at low gravity obtained by using intense back lighting. Number of the frame in the motion picture sequence is shown in the corner of each photograph. For heptane $d_0 = 0.5$ mm and for toluene $d_0 = 0.46$ mm. Framing rate = 250 frames per second. The black camera marker at the top of each picture is fixed to the moving frame of reference. The emergence of the right electrode is shown in (*a*) as the droplet drifts during free fall.

(*Facing p.* 192)

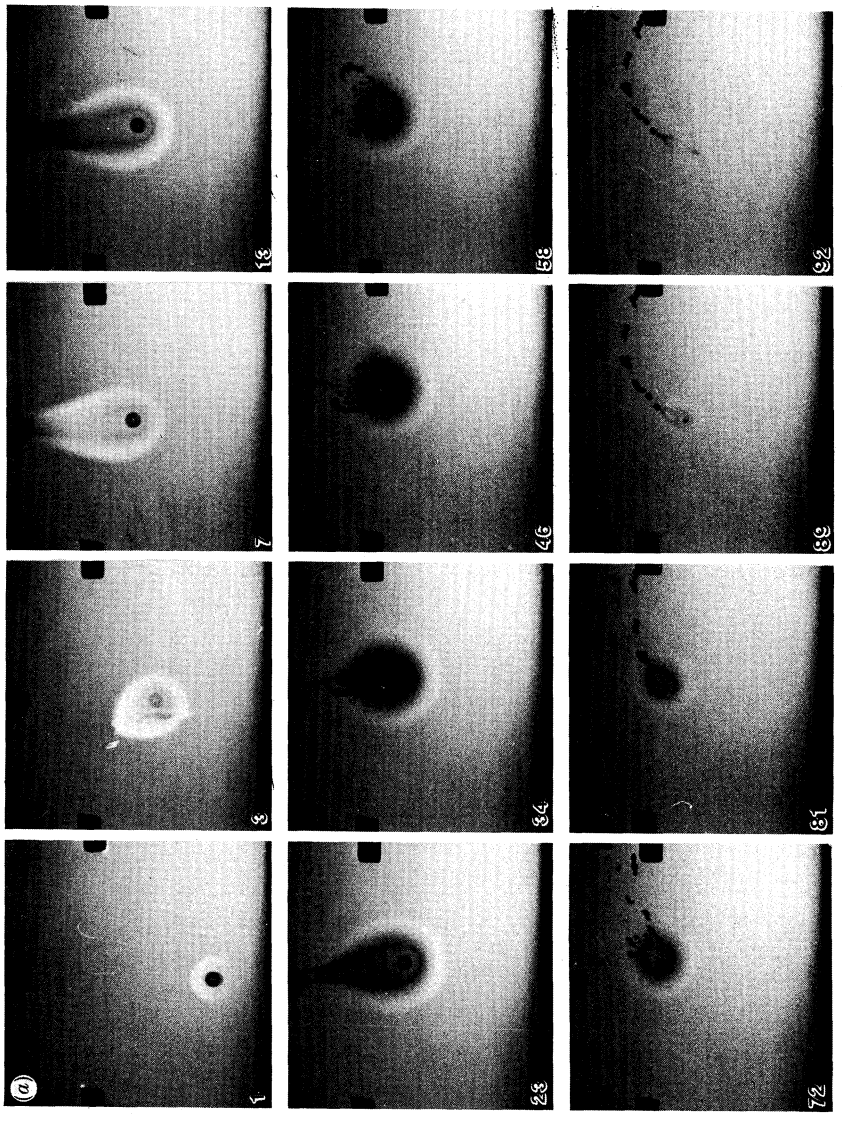

FIGURE 9*a*. For description see opposite.

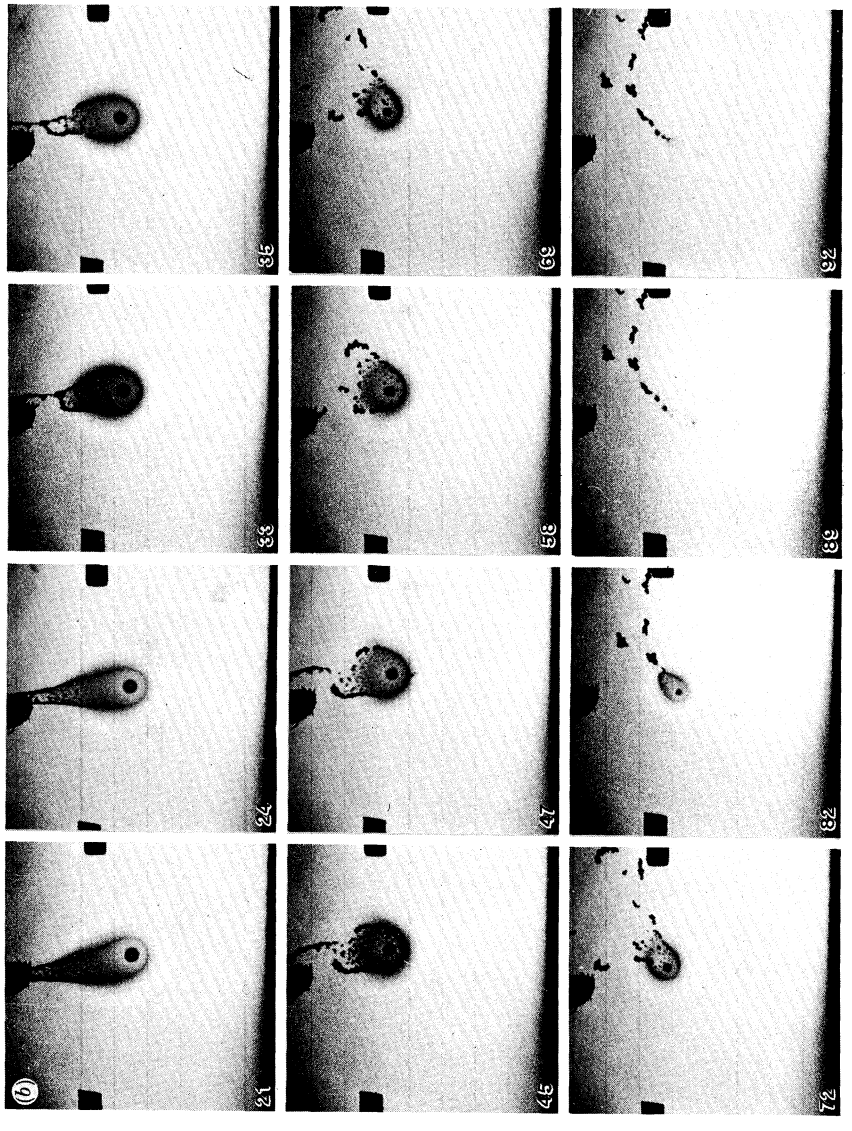

FIGURE 9. The flame shape around a toluene droplet burning at low gravity. Number of frame in the motion picture sequence is shown in the corner of each photograph. The droplet is rising to its apex in frame 1, and is in free-fall in frame 3 after which it is nearly stationary. Electrodes (the moving frame of reference) are visible in the pictures. Figure 9*a* shows low contrast photographs to illustrate the luminous zone of the flame around the droplet. The higher contrast sequences shown in figure 9*b* (the same droplet as in (*a*)) illustrate the carbon or soot ring around the burning droplet. Framing rate = 250 frames per second and $d_0 = 0.44$ *mm*.

high (figure 9*b*, plate 3) contrast paper, respectively. The number below each picture represents the relative position of that picture in the entire photographic sequence, and the camera framing rate was 250 frames per second. Visible on the either side of each frame are the electrodes. The droplet that is in free fall remained nearly at the midplane between the electrodes, also in free fall, throughout burning.

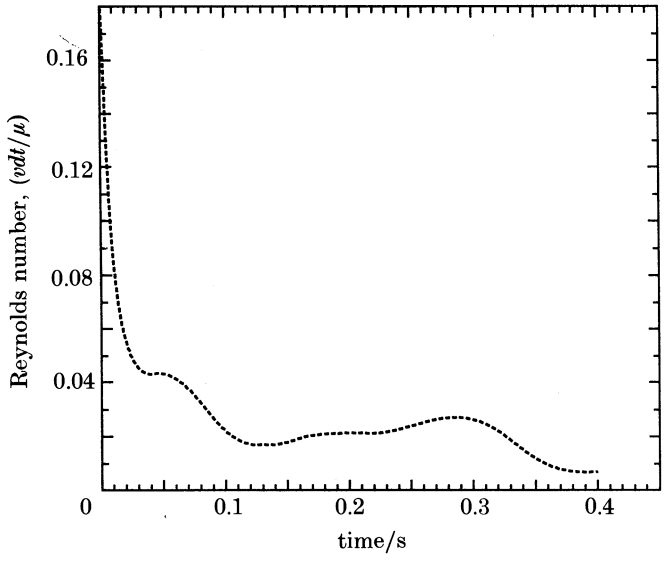

FIGURE 7. Evolution of free-stream Reynolds number around the heptane droplet shown in figure 6*a*. Effective free-stream flow is caused by droplet motion. Air properties were taken from Incropera & DeWitt (1981).

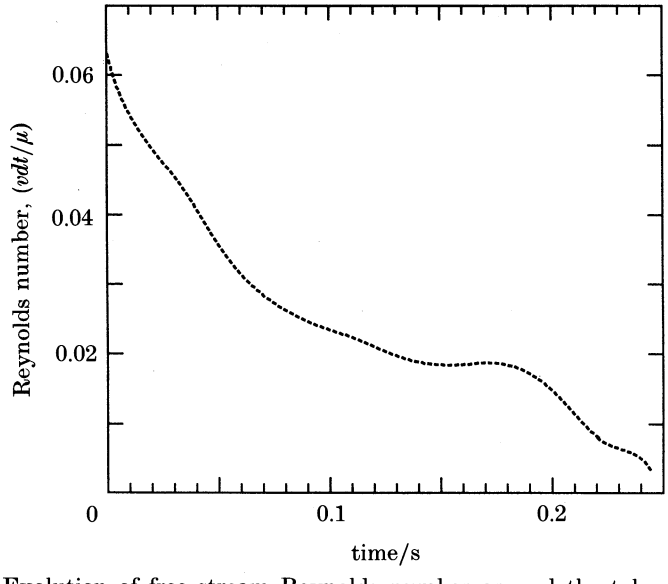

FIGURE 8. Evolution of free stream Reynolds number around the toluene droplet shown in figure 6*b*. Effective free-stream flow is caused by droplet motion. Air properties were taken from Incropera & DeWitt (1981).

Two zones of luminosity exist around the droplet, one defined by an outer region, which probably defines the primary reaction zone of the flame, and the other characterized by the appearance of a ring of what may be carbon or soot between the droplet surface and the outer region. The shape of the outer luminous zone is nearly spherical when the droplet motion ceases (after the 13th frame) whereas the carbon zone exhibits a tail that extends across the outer zone boundary and then breaks up as it collapses into a spherical shape.

The carbon or soot ring is more clearly illustrated in the series of higher contrast photographs in figure 9*b*. As the droplet slows to a halt, the carbon zone attempts to collapse into a spherical shape to reflect the reduction of axial gas movement around the droplet. The forward hemisphere achieves a nearly spherical shape (frames subsequent to the 35th frame), whereas the structure of the carbon trail in the wake breaks up during the collapse (frame 45 and beyond).

The origin of the carbon around the droplet shown in figure 9 could be related to the complex chemical kinetics that can cause hydrocarbon fuels to produce soot. The structure and geometry of the carbon ring around the droplet, though, may be dependent on the magnitude of the axial vapour flow around the droplet, whether induced by buoyancy or created by movement of the droplet. The magnitude of the heat transfer rate to the droplet may be dependent on the geometry of the carbon ring. Variations in the magnitude of the velocity of the droplet before or after ignition could then produce variations in the droplet burning rate from run to run.

A carbon ring around a free floating *n*-decane droplet burning in air under low gravity was also observed in a prior study (Shaw *et al.* 1987). In that study the carbon or soot shell moved progressively closer to the droplet as burning progressed until it apparently collapsed on the droplet surface at which time the droplet exploded. Such explosions are reminiscent of the vapour explosions which can occur when a cold liquid is rapidly heated by sudden contact with a hot solid surface. If the liquid adjacent to the solid surface is heated faster than the time it takes a bubble activated at a nucleation 'site' at the surface to grow and thereby to control the phase transition, the liquid can reach its superheat limit (Avedisian 1985). At this limit, the phase change can be explosive. The mechanism for such an intrinsic phase transition is homogeneous nucleation (Reid 1983). Droplet explosions were not observed in the present set of experiments because the carbon ring disintegrated (cf. frames 33–69 in figure 9*b*) before making contact with the droplet. Such disintegration may be initiated by the (however low in magnitude) movement of the droplet, which for the sequence shown in figure 9 was almost nil as evidenced by the position of the droplet relative to the camera marker and electrodes.

Figures 10 and 11 illustrate the evolution of the square of droplet diameter in dimensional form for the heptane and toluene droplets illustrated in figure 6. The diameter decreased monotonically with time and either disappeared (toluene) or reached a constant value (heptane). In the initial period immediately after ignition the droplet diameter was nearly constant. This fact is characteristic of a transient heating period. The extent of this period is small and occupied less than 10% of the total burning sequence.

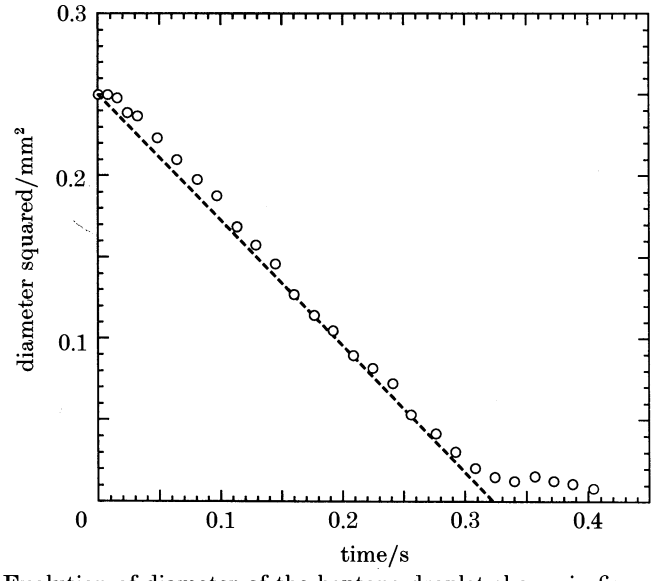

FIGURE 10. Evolution of diameter of the heptane droplet shown in figure 6*a*. The broken line is the prediction from equation (1). Properties used in the calculations are listed in table 1.

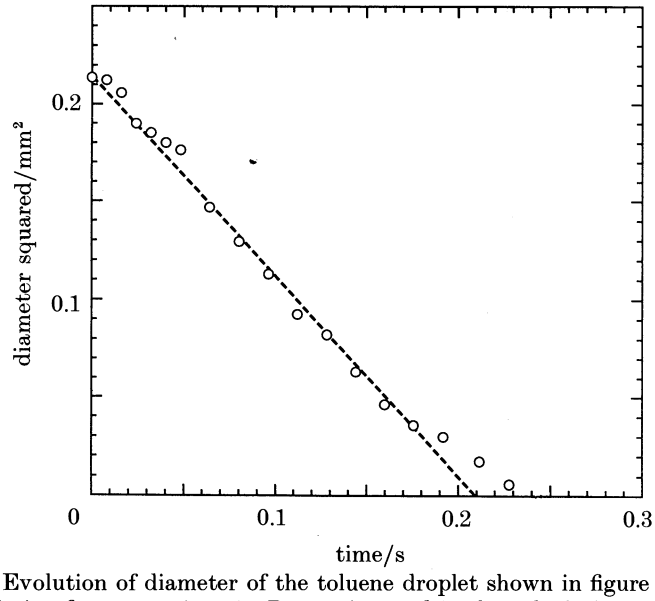

FIGURE 11. Evolution of diameter of the toluene droplet shown in figure 6*b*. The broken line is the prediction from equation (1). Properties used in the calculations are listed in table 1.

Extinction was believed to be manifested by a period near the end of the monotonic decrease in droplet diameter beyond which the droplet diameter did not change, as suggested from previously performed suspended droplet experiments carried out at $g/g_0 = 1$ (Chung & Law 1986). Extinction was most pronounced for heptane as shown in figure 10, and to a much lesser extent for toluene (figure 11).

It is conjectured that extinction was not the result of quenching of the flame by heat transfer to the electrodes due to the proximity of the droplet to the electrode shown in figure 6 because it has also been observed in subsequent experiments for other droplets which remained positioned nearly at the midpoint between the electrodes throughout burning. A more plausible mechanism for extinction under low gravity could be blanketing of the flame by the combustion products thus starving the reaction zone of oxygen (Carleton & Weinberg 1987), or the chemical reactions at the flame front occurring at finite rates (Chung & Law 1986). Without benefit of an axial vapour flow around a droplet to assist in directing the combustion products away from the flame, the lingering of these products around the droplet could provide a barrier to the diffusion of oxygen that is required to sustain the flame. Also, fuel leakage through the reaction zone attendant to finite reaction rates may lower the flame temperature, leading to a further lowering of the reaction rates and eventual extinction.

The earliest theories of droplet burning were based on the assumption of complete spherical symmetry (Godsave 1953; Spalding 1953). They further assumed that properties were constant and that transient heating processes within the droplet were neglected. The droplet was considered to be at its wet bulb temperature at the instant of ignition. These theories lead to the well-known 'd^2' law, namely that the rate of change of the square of the droplet diameter was a constant. In non-dimensional form, this result is the following:

$$\mathrm{d}D^2/\mathrm{d}\tau = -K, \tag{1}$$

where the burning rate 'constant' is

$$K = 8\ln(1+B) \tag{2}$$

and the transfer number B is defined as

$$B = [C_{\mathrm{p}}(T_{\mathrm{b}}-T_{\infty})+QY_{\mathrm{o}\infty}v_{\mathrm{f}}W_{\mathrm{f}}/v_{\mathrm{o}}W_{\mathrm{o}}]/h_{\mathrm{fg}}. \tag{3}$$

A one-step chemical reaction at the flame front in the form

$$v_{\mathrm{f}}\,\mathrm{fuel}+v_{\mathrm{o}}\,\mathrm{O}_2 \rightarrow \mathrm{products}$$

is characteristically assumed to obtain equation (1). The flame shape that emerges from this theory is spherical and, when normalized by the droplet diameter, is predicted to be a constant.

Modifications to equation (2) that account for axial vapour flow around a droplet, whether induced by free or forced convection, have been proposed in the following form (Law & Williams 1972):

$$K = 8\ln(1+B)(1+f_1)(1+f_2), \tag{4}$$

where

$$f_1 = a\,Re_0^b\,D^b, \tag{5}$$

$$f_2 = c\,Gr_0^e\,D^{3e} \tag{6}$$

and a, b, c, and e are empirical constants.

Previous analyses have established the theoretical foundation of equation (4) in the Stokes flow régime ($Re_0 \ll 1$) when $Gr_0 = 0$. The result was that $a = 0.25$

and $b = 1$ (Fendell *et al.* 1966; Gogos *et al.* 1986). A best fit of some suspended and free droplet burning data at higher Reynolds numbers yielded $a = 0.276$, $b = 0.5$, $c = 0.533$, and $e = 0.52$ (Frossling 1938; Law & Williams 1972). A form like equation (4) will not yield substantially different predictions than equation (2) when $Re_0 \ll 1$ and $Gr_0 \ll 1$ (actually, $Gr_0 \sim 10^{-5}$ when $g/g_0 \sim 0.001$ as in the present experiments), both limits of which apply to the present data. In these limits, $f_1 \ll 1$ and $f_2 \ll 1$. A numerical integration of equation (1) that used either (2) or (4) for the burning rate revealed differences in the predicted droplet diameter that were smaller than the precision of the experimental uncertainty in the measurements (about the width of the symbols in figures 10 and 11). It is therefore questionable whether or not meaningful comparisons can be made between a low Reynolds number theory for droplet combustion and measured droplet diameter data because of both the precision of the measurements and the relatively small effect of a stokesian flow on the predicted diameter.

The solid lines in figures 10 and 11 are based on equations (1) and (2). The calculations were found to be sensitive to the physical property values, in particular the vapour thermal conductivity and vapour specific heat, which appear in the definition of τ. Deviations from the recommended procedure for estimating physical properties (Law & Williams 1972) consisted of using a hydrocarbon mole fraction x of 0.2 rather than the suggested value of 0.4 to evaluate the mole fraction average of the hydrocarbon and air gas-phase thermal conductivity around a heptane droplet (i.e., $k_g = xk_{g\,\mathrm{heptane}} + (1-x)\,k_{g\,\mathrm{air}}$), and using a mole fraction average of the air and toluene specific heat to estimate the gas phase specific heat around a burning toluene droplet (assuming $x = 0.4$ for toluene) rather than taking $C_p = C_{p\,\mathrm{toluene}}$ as recommended. These *ad hoc* constructions yielded the agreement with measured droplet diameters shown in figures 10 and 11. Other choices yielded poorer agreement. A summary of the property values used in the calculations is provided in table 1. The ideal gas specific heat and the thermal conductivity (calculated by using the Roy–Thodos method) of heptane and toluene were taken from Reid *et al.* (1977). The properties of air were taken from the compilation of Incropera & DeWitt (1981). Liquid densities and heats of vaporization were obtained from Vargaftik (1975).

TABLE 1. PROPERTY VALUES[a]

	heptane	toluene
C_p/(cal g^{-1} K^{-1})[b]	1.02 (1338)	0.74 (1342)
ρ_l/(g cm^{-3})	0.614 (372)	0.78 (384)
h_{fg}/(cal g^{-1})	75.6 (372)	87.0 (384)
k_g/(cal cm^{-1} s^{-1} K^{-1})	5.46×10^{-4} (1338)	2.20×10^{-4} (1342)
Q/(cal g^{-1})	10620	9780
T_b/K	371.6	383.8
W_f/(g gmol^{-1})	100.205	92.141
β/K^{-1}	7.47×10^{-4} (1338)	7.45×10^{-4} (1342)
v_f	1	1
v_o	11	9

[a] The number in parenthesis is the temperature (in kelvins) at which the property was evaluated.

[b] 1 calorie (thermochemical) = 4.184 J.

The perspective within which the low-gravity unsupported droplet burning data obtained here can be placed in light of previously reported free droplet data obtained under similar conditions is shown in figure 12. Compared in figure 12 are the present free droplet data with those previously reported by Okajima & Kumagai (1975). The measurements are displayed in non-dimensional form to suppress the effects of initial droplet diameter; $x = 0.2$ was used to evaluate the vapour thermal conductivity and $C_p = C_{p\,\mathrm{fuel}}$ was assumed to evaluate the specific heat (Law & Williams 1972) in the definition of τ. Agreement is quite favourable with the differences being within experimental uncertainty. A larger fraction of the droplet burning time (indeed 100% of it) that is accessible by the technique described in §3 is clearly revealed. Yet it is interesting to note that the low-gravity burning rate for heptane measured by data that spanned only a limited portion of the total burning time was reported to be 0.78 $\mathrm{mm^2\,s^{-1}}$ (Okajima & Kumagai 1975), whereas the burning rate obtained from the data shown in figure 10 which spanned the complete history of burning was 0.79 $\mathrm{mm^2\,s^{-1}}$. In the determination of these burning rate constants, represented essentially by the derivative of the evolution of d^2 with time, data that were obtained during the droplet heating period were excluded. These data were the first three points for each of the free droplet data sets displayed in figure 12.

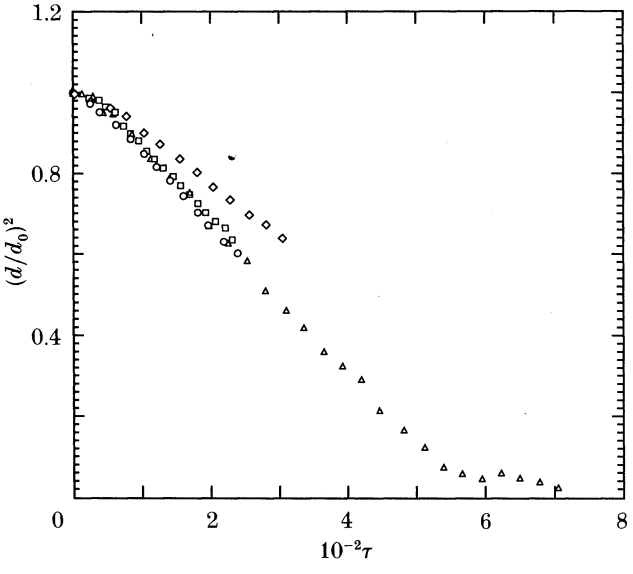

FIGURE 12. Comparison between the present heptane data (△, $d_0 = 0.5$ mm) with those reported by Kumagai *et al.* (1971) for a fibre-mounted droplet ($d_0 = 0.96$ mm: □, 45° line; ◇, lateral dimension) and Okajima & Kumagai (1975) for a free droplet (○, $d_0 = 1.33$ mm). Data are displayed in non-dimensional form to suppress the effects of initial droplet size; $\tau \equiv (tk_g/\rho_l c_p d_0^2)$.

Finally, shown in figure 12 is a comparison between the measured evolution of droplet diameter for a fibre-mounted heptane droplet (Kumagai *et al.* 1971) and the free droplet data reported here and elsewhere (Okajima & Kumagai 1975). Depending on how the diameter of a fibre-mounted droplet is defined, the

agreement can be quite favourable or poor. The problem is that the shape of a droplet suspended from a fibre will be distorted from the spherical because of the action of surface tension. The distortion becomes more pronounced as burning progresses because the droplet diameter approaches the fibre diameter. Two measures of the droplet dimension yielded the results displayed in figure 12. An effect of the fibre can be argued if the droplet diameter is taken simply as the lateral droplet diameter, whereas defining the diameter based on the 45° line used by Okajima & Kumagai (1975) yields results that are essentially indistinguishable from the free droplet data. Thus, any agreement claimed between free and suspended droplet burning data may be fortuitous to the extent that such agreement will depend on how the effective diameter of a fibre-supported droplet is defined. The droplet shape, though, apparently has a less pronounced effect on the flame shape under low gravity in that the flame appears to retain a spherical shape even when the droplet shape is affected by the fibre.

This work was supported by the Department of Energy, Office of Basic Energy Sciences–Engineering Research Program, which is under the direction of Dr Oscar P. Manley, through contract no. DE-AC02-83ER13092. This work could not have been undertaken without this financial support. Additional support has been obtained from the National Science Foundation under grant no. CBT-8451075, for which we are also grateful.

References

Avedisian, C. T. 1985 *J. Phys. Chem. Ref. Data.* **14**, 695–729.
Brzustowski, T. A., Twardus, E. M., Wojcicki, S. & Sobiesiak, A. 1979 *AIAA Jl* **17**, 1234–1242.
Brzustowski, T. A., Sobiesiak, A. & Wojcicki, S. 1981 In *18th Symp.* (*Int.*) *Comb.*, pp. 265–273.
Carleton, F. B. & Weinberg, F. J. 1987 *Nature, Lond.* **330**, 635–636.
Chung, S. H. & Law, C. K. 1986 *Combust. Flame.* **64**, 237–241.
Faeth, G. M., Dominicis, D. P., Tulpinsky, J. F. & Olson, D. R. 1969 In *12th Symp.* (*Int.*) *Comb.*, pp. 9–18.
Fendell, F. E., Sprankel, M. L. & Dodson, D. S. 1966 *J. Fluid Mech.* **26**, 267–280.
Frossling, N. 1938 *Beitr. Geophys.* **52**, 170–216.
Gieras, M., Klemens, R. & Wojcicki, S. 1985 *Acta astronaut.* **12**, 573–579.
Gieras, M., Klemens, R. & Wolanski, P. 1986 *Acta astronaut.* **13**, 231–239.
Godsave, G. A. E. 1953 In *4th Symp.* (*Int.*) *Comb.*, pp. 818–830.
Gogos, G., Sadhal, S. S., Ayyaswamy, P. S. & Sundararajan, T. 1986 *J. Fluid Mech.* **171**, 121–144.
Incropera, F. P. & DeWitt, D. P. 1981 *Introduction to heat transfer*, p. 681. New York: John Wiley & Sons.
Isoda, H. & Kumagai, S. 1959 In *7th Symp.* (*Int.*) *Comb.*, pp. 523–531.
Kimura, M., Ihara, H., Okajima, S. & Iwama, A. 1986 *Combust. Sci. Technol.* **44**, 289–306.
Knight, B. & Williams, F. A. 1980 *Combust. Flame.* **38**, 111–119.
Kumagai, S. 1956 *Jet Propul.* **26**, 7.
Kumagai, S. & Isoda, H. 1957 In *6th Symp.* (*Int.*) *Comb.*, pp. 726–731.
Kumagai, S., Sakai, T. and Okajima, S. 1971 In *13th Symp.* (*Int.*) *Comb.*, pp. 779–785.
Law, C. K. & Williams, F. A. 1972 *Combust. Flame.* **19**, 393–405.
Lazar, B. S. & Faeth, G. M. 1971 In *13th Symp.* (*Int.*) *Comb.*, pp. 801–811.
Okajima, S., Kanno, H. & Kumagai, S. 1985 *Acta. astronaut.* **12**, 555–563.

Okajima, S. & Kumagai, S. 1975 In *15th Symp.* (*Int.*) *Comb.*, pp. 401–407.
Okajima, S. & Kumagai, S. 1982 In *19th Symp.* (*Int.*) *Comb.*, pp. 1021–1027.
Reid, R. C. 1983 *Adv. Chem. Engng*, **12**, 105–208.
Reid, R. C., Prausnitz, J. M. & Sherwood, T. K. 1977 *Properties of gases and liquids*, 3rd edn. New York: McGraw-Hill.
Shaw, B. D., Dryer, F. L., Williams, F. A. & Haggard, J. B. 1987 Paper No. IAF-87-403, International Astronautical Congress, Brighton, England, 10–17 October.
Spalding, D. B. 1953 In *4th Symp.* (*Int.*) *Comb.*, pp. 847–864.
Vargaftik, N. B. 1975 *Handbook of physical properties of liquids and gases*, 2nd edn. New York: Hemisphere Publishing Co.
Wang, C. H. 1983 Ph.D. thesis, Northwestern University.
Yang, J. C. 1988 Ph.D. thesis, Cornell University. (In preparation.)

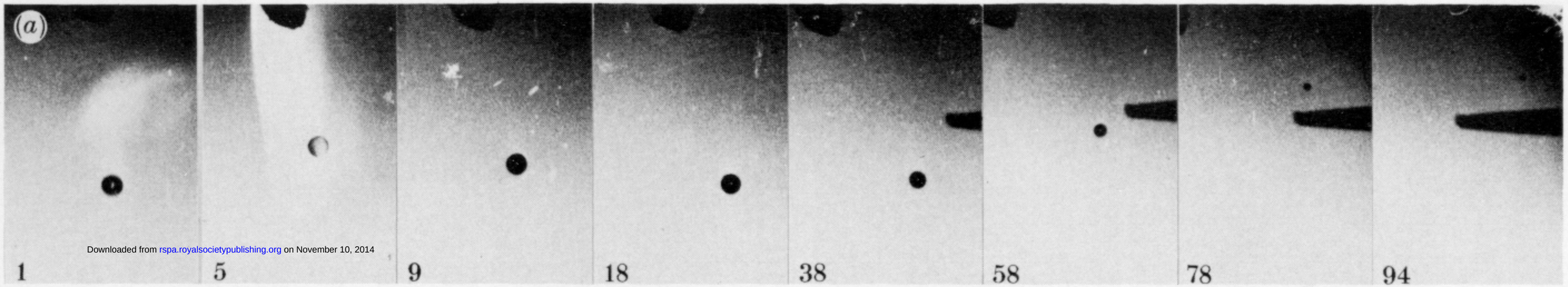

FIGURE 6. Photographic sequences of a burning and free-falling heptane (a) and toluene (b) droplet at low gravity obtained by using intense back lighting. Number of the frame in the motion picture sequence is shown in the corner of each photograph. For heptane $d_0 = 0.5$ mm and for toluene $d_0 = 0.46$ mm. Framing rate = 250 frames per second. The black camera marker at the top of each picture is fixed to the moving frame of reference. The emergence of the right electrode is shown in (a) as the droplet drifts during free fall.

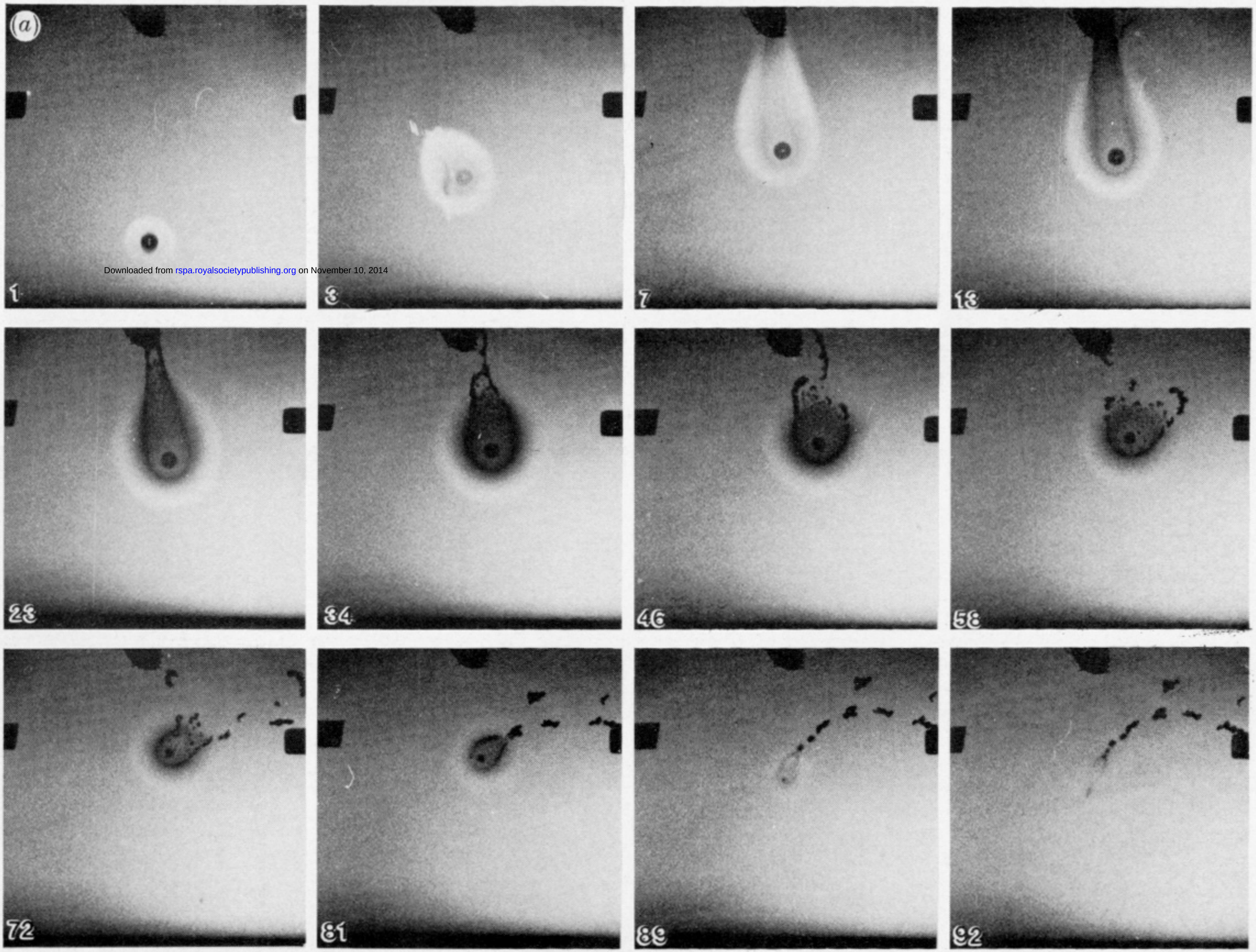

FIGURE 9*a*. For description see opposite.

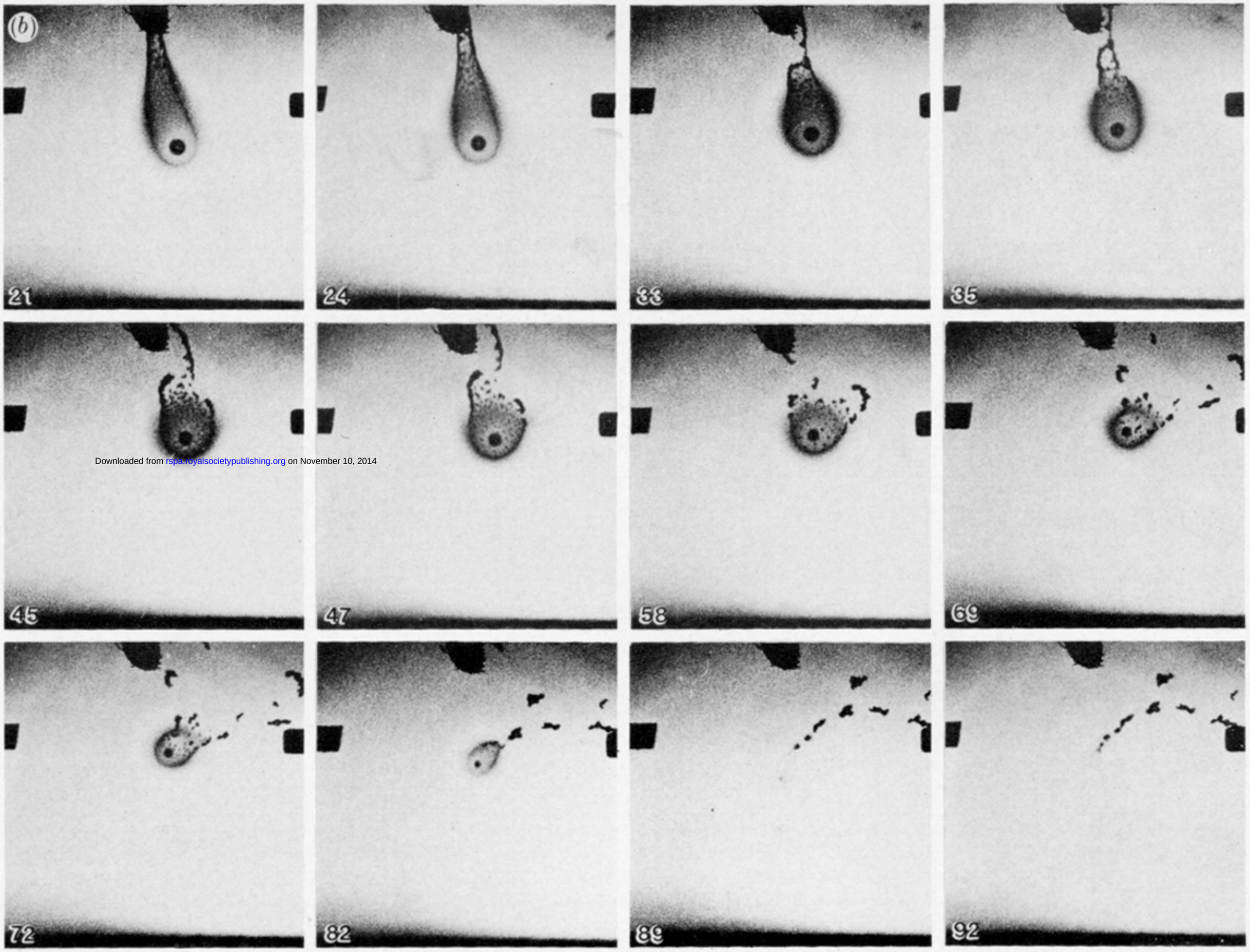

FIGURE 9. The flame shape around a toluene droplet burning at low gravity. Number of frame in the motion picture sequence is shown in the corner of each photograph. The droplet is rising to its apex in frame 1, and is in free-fall in frame 3 after which it is nearly stationary. Electrodes (the moving frame of reference) are visible in the pictures. Figure 9*a* shows low contrast photographs to illustrate the luminous zone of the flame around the droplet. The higher contrast sequences shown in figure 9*b* (the same droplet as in (*a*)) illustrate the carbon or soot ring around the burning droplet. Framing rate = 250 frames per second and $d_0 = 0.44$ mm.